

The Quiescent X-Ray Spectrum of the Neutron Star in Cen X-4 Observed with *Chandra*/ACIS-S

Robert E. Rutledge^{1,6}, Lars Bildsten², Edward F. Brown³, George G. Pavlov^{4,6},
and Vyacheslav E. Zavlin^{5,6}

ABSTRACT

We report on spectral and intensity variability analysis from a *Chandra*/ACIS-S observation of the transient, type-I X-ray bursting low-mass X-ray binary Cen X-4. The quiescent X-ray spectrum during this observation is statistically identical to one observed previously with *BeppoSAX*, and close, but not identical, to one observed previously with *ASCA*. The X-ray spectrum is best described as a pure Hydrogen atmosphere thermal spectrum plus a power-law component that dominates the spectrum above 2 keV. The best-fit radius of the neutron star is $r = 12.9 \pm 2.6$ ($d/1.2$ kpc) km if the interstellar absorption is fixed at the value implied by the optical reddening. Allowing the interstellar absorption to be a free parameter yields $r = 19_{-10}^{+45}$ ($d/1.2$ kpc) km (90% confidence). The thermal spectrum from the neutron star surface is inconsistent with a solar metallicity. We find a 3σ upper-limit of root-mean-square variability $\leq 18\%$ (0.2-2.0 keV; 0.0001-1 Hz) during the observation. On the other hand, the 0.5-10.0 keV luminosity decreased by $40 \pm 8\%$ in the 4.9 years between the *ASCA* and *Chandra* observations. This

¹ Space Radiation Laboratory, California Institute of Technology, MS 220-47, Pasadena, CA 91125; rutledge@srl.caltech.edu

² Institute for Theoretical Physics and Department of Physics, Kohn Hall, University of California, Santa Barbara, CA 93106; bildsten@itp.ucsb.edu

³ Enrico Fermi Institute, University of Chicago, 5640 South Ellis Ave, Chicago, IL 60637; brown@flash.uchicago.edu

⁴ The Pennsylvania State University, 525 Davey Lab, University Park, PA 16802; pavlov@astro.psu.edu

⁵ Max-Planck-Institut für Extraterrestrische Physik, D-85740 Garching, Germany; zavlin@xray.mpe.mpg.de

⁶ Institute for Theoretical Physics, Kohn Hall, University of California, Santa Barbara, CA 93106

variability can be attributed to the power-law component. Moreover, we limit the variation in thermal temperature to $\lesssim 10\%$ over these 4.9 years. The stability of the thermal temperature and emission area radius supports the interpretation that the quiescent thermal emission is due to the hot neutron star core.

Subject headings: stars: neutron — stars: individual (Cen X–4)

1. Introduction

Measuring both the mass (M) and the radius (R) of a neutron star (NS) would strongly constrain the nuclear equation of state. To distinguish between the competing models, several measurements of a few percent accuracy in M and R are required. While the masses of several NSs have been constrained to 10% or better (see Thorsett & Chakrabarty 1999 for a recent review) from pulsar timing of Doppler shifts, measuring the NS radii has proven to be difficult. There are at least five ways to measure R using X-ray emission from accreting NSs: (1) the spectral evolution of radius-expansion type-I X-ray bursts; (2) the measurements of M/R from the gravitational red-shift of metallic spectral lines during type I X-ray bursts or γ -ray lines during accretion; (3) inferring constraints from NS kHz quasi-periodic oscillations; (4) pressure broadening and red-shift of photospheric metal lines; and (5) spectral analysis of transiently accreting NSs in quiescence.

Efforts to measure the NS radius through the spectral evolution of radius-expansion type-I X-ray bursts (for a review, see Lewin et al. 1993) based on theoretical non-Planckian spectra (Van Paradijs 1982; London et al. 1986; Pavlov et al. 1991; Madej 1991; Titarchuk 1994) have been somewhat successful. Performing this measurement with the emission from a type-I X-ray burst has the advantage that the observed luminosity originates from the NS photosphere and not the surrounding accretion disk. The measured NS radii range from 6 to 15 km. The reliability of these measurements is limited by systematic uncertainties in the emergent spectrum, the fraction of the NS surface area involved in the burst and the elemental composition of the photosphere, as well as the distance to the NS (Van Paradijs & Lewin 1987; Damen et al. 1989; Damen et al. 1990).

Attempts to measure NS photospheric metal lines as expected from model atmospheres (Foster et al. 1987) have had mixed success. Absorption lines observed in the tails of type-I X-ray bursts (Waki et al. 1984; Nakamura et al. 1988; Magnier et al. 1989) have not been confirmed through repeated observation with more sensitive instrumentation, resulting in metallicity limits of $Z < 0.4Z_{\odot}$ (Day et al. 1992). Moreover, the interpretation of these lines as due to absorption in the photosphere is in doubt (Madej 1990). Repeated observations

of such lines, and their identification with a known transition would measure M/R . Gamma-ray lines from the accretion process are also a possibility (Bildsten et al. 1992; Bildsten et al. 1993), though the levels of emission are still below the ability of current instruments.

Observations of kilo-Hz quasi-periodic oscillations from accreting neutron stars, interpreted as the orbital period at or above the marginally stable orbit (Kluźniak et al. 1990; Kaaret et al. 1997; Kluźniak 1998) have been used to constrain both M and R using observations from eight accreting neutron stars, finding $M \approx 2M_{\odot}$ (Zhang et al. 1997). The NS radius is then less than the marginally stable orbit for a mass of this size (<18 km for a non-rotating star).

Another method of measuring R for a slowly rotating NS is the approach described by Paerels (1997), with metal lines from an emergent NS X-ray spectrum. Measuring the pressure broadening ($\propto M/R^2$) and photospheric red-shift ($\propto M/R$) yields both M and R . This method is intriguing because it is *independent of distance*, which can be uncertain by up to a factor of 2 in the isolated transient NSs, although it can be determined to $\approx 5\%$ for the low-luminosity X-ray sources in globular clusters (Hertz & Grindlay 1983; Verbunt et al. 1984). Once several metal lines are identified in the photospheric spectrum, this method is very likely to provide a number of M and R measurements.

To these approaches has recently been added a new means of measuring R with X-ray spectroscopic observations of transiently accreting, low magnetic-field ($<10^{10}$ G) NSs in quiescence (Brown et al. 1998; Rutledge et al. 1999; Rutledge et al. 2000). Until this work, the spectral observations had been interpreted as black-body radiation (Van Paradijs et al. 1987; Garcia 1994; Verbunt et al. 1995; Asai et al. 1996b; Asai et al. 1998; Campana et al. 1998b; Garcia & Callanan 1999; Campana et al. 2000), yielding effective temperatures of $kT_{\infty}=0.2-0.3$ keV. For most sources, the thermal component has a black-body emission area radius much smaller than a NS ($\lesssim 1$ km).

As described by Brown, Bildsten & Rutledge (1998, BBR98 hereafter), a black-body spectrum is not appropriate for weakly magnetic⁷ transiently accreting NSs with $kT_{\text{eff}} < 5 \times 10^6 K$. At accretion rates $\ll 10^{12} \text{g s}^{-1}$ the accreting metals gravitationally settle faster than they are supplied, and the atmosphere is nearly pure hydrogen (Bildsten et al. 1992). The dominant opacity is free-free absorption ($\propto \nu^{-3}$) which results in a spectrum in which higher energy photons escape from deeper in the NS atmosphere, where the temperature is higher (Pavlov & Shibanov 1978; Rajagopal & Romani 1996; Zavlin

⁷In low magnetic field NSs ($\leq 10^{10}$ G), the magnetic field plays no role in determining the opacity of the atmosphere at energies above 0.1 keV, and thus can be neglected (Zavlin et al. 1996).

et al. 1996). This hardens the spectrum which, (mis-)interpreted as a black-body, results in systematically higher temperatures and *lower* emission area radii. When the *ASCA* and *ROSAT* observations are fit with the more appropriate thermal H atmosphere spectrum, the emission area radii are ≈ 10 km (Rutledge et al. 1999; Rutledge et al. 2000), confirming that this emission is mostly thermal. These objects have thus become the focus of our efforts to measure the NS surface area.

If the emission area radius of the thermal part of the quiescent X-ray spectrum is the NS radius, it should be constant from observation to observation. In addition, if accretion onto the NS makes no contribution to the quiescent luminosity, the temperature should also be constant on timescales $\ll 10^6$ yrs, the core cooling timescale (see Ushomirsky & Rutledge 2001 for exceptions). In the most sensitive observations, an additional power-law component is observed above a few keV (Asai et al. 1996b; Asai et al. 1998; Campana et al. 1998b; Campana et al. 2000). If produced through interaction between the accretion and magnetosphere (Campana et al. 1998b), it might vary on short (\sim msec) timescales, and perhaps show a pulsation at the NS spin frequency.

In this paper, we present X-ray spectroscopic analysis of Cen X–4 in quiescence. Cen X–4 is a transient, type-I X-ray bursting low-mass X-ray binary (for reviews on transients, see Tanaka & Lewin 1995; Tanaka & Shibazaki 1996; Chen et al. 1997). Its distance is estimated to be 1.2 ± 0.3 kpc on the basis of two observed radius-expansion bursts (Chevalier et al. 1989); formally, this is a distance upper-limit. It is in a $P_{\text{orb}} = 0.629$ day binary with a K dwarf (Chevalier et al. 1989; McClintock & Remillard 1990), and has been observed in outburst twice (1969 and 1979; see discussion in § 3.1). We compare the observed X-ray spectrum with a number of models, in particular with the H atmosphere model. We also compare the spectrum with spectra of the same source in archived observations. We place limits on changes in the thermal spectrum of the NS on year long timescales. In §2, we present the analysis of the *Chandra* data. In §2.3, we compare the *Chandra* data with past observations, and characterize the spectral differences between this and past X-ray observations. We discuss these results and their implications for this and other sources and conclude in §3.

2. Observation and Analysis

The observation occurred 23 Jun 2000 01:23:01-04:32:54 TT for a total exposure time of 9561.4 seconds with *Chandra*/ACIS-S3 (backside illuminated). The source position was aimed $4'$ off-axis, with a $1/8$ subarray used with 0.4 sec exposures. The time between successive frames was 0.44104 sec, which gives $\approx 10\%$ dead-time. We analyzed data from

the pre-processed Level 2 FITS data provided with the standard data products. The X-ray source appears at the known optical position of Cen X-4 ($\pm 1''$; Canizares et al. 1980). Only one other point source (previously unknown) was found in the field with the *Chandra* Interactive Analysis of Observations Software (CIAO) point-source detection tool *celldetect*⁸, with a S/N of 3.5, roughly $1'$ away.

We extracted data from a circle 10 pixels in radius about the Cen X-4 X-ray source position, and background from an annulus with inner and outer radius of 13 and 50 pixels, respectively. There were a total of 2714 good counts in the source region, and 575 in the background region; we expect 25 background counts in the source region ($\approx 1\%$ of the total counts in the source region).

2.1. *Chandra* Spectral Analysis

The temperature of the focal-plane instruments has been decreased during *Chandra*'s lifetime; this alters the energy response of the ACIS-S chips. The data were taken with a focal-plane chip temperature of -120C , and we used the corresponding response files for this temperature, according to the standard ACIS-S analysis.

We binned the photons between 0.5 and 1.5 keV into bins of width ≈ 130 eV wide, comparable to the energy resolution (FWHM) in the BI-S3 detector. Above 1.5 keV, we binned the data so that there were 40 counts per bin (wider than the spectral resolution). We used spectral data in the energy range 0.5-10 keV. While there are significant counts below 0.5 keV, the ACIS-S energy calibration is presently not reliable below this energy; we will re-examine this analysis when the energy calibration is refined below 0.5 keV. In addition, the current *Chandra* response files for the ACIS-S-BI underestimate the detector area by up to 20% near 0.5 keV (N. Schulz, priv. comm.). To account for the calibration uncertainties, we included a 25% systematic uncertainty in the 0.5-0.6 keV energy range, and a 5% systematic uncertainty in 0.6-0.7 keV energy range. This is in addition to a 4% systematic uncertainty across all energies that accounts for other calibration uncertainties.

We fit the data in XSPEC v11 (Arnaud 1996), with several spectral models (powerlaw, H atmosphere, blackbody, Raymond-Smith, or thermal bremsstrahlung), all with galactic absorption (N_{H}) as a free parameter, except where noted. The H atmosphere spectrum is not a standard XSPEC model, but has been described and calculated elsewhere (Zavlin et al. 1996). The hydrogen column density for Cen X-4 was estimated during quiescence

⁸available at <http://asc.harvard.edu>

to be $N_{\text{H},22} < 0.20$ (Asai et al. 1996a; $N_{\text{H}} = 10^{22} N_{\text{H},22} \text{ cm}^{-2}$); its optical reddening is $E(B - V) = 0.1$ (Blair et al. 1984). These values are consistent with an approximate optical reddening/hydrogen column density ratio found from observing the halos of X-ray sources (Gorenstein 1975; Predehl & Schmitt 1995), which imply an equivalent hydrogen column density of $N_{\text{H},22} = 0.055$.

No single component model fit the data acceptably (prob $\ll 10^{-6}$). In the black-body and H atmosphere fits, the high-energy (> 2 keV) powerlaw spectral component reported previously (Asai et al. 1996b; Campana et al. 2000) is apparent. In general, the single component models failed due to the presence of this high-energy component. We then fit the data with two-component models, where the second component is a power-law that accounts for the > 2 keV emission. The best-fit absorbed H atmosphere spectrum has parameters listed in Table 1. We also provide the best fit parameters with N_{H} held fixed at the optically implied value ($N_{\text{H},22} = 0.055$), and the resulting intrinsic (that is, unabsorbed) spectrum in Figure 1.

While a double power-law model was statistically acceptable, the low energy component has a steep power-law slope (photon index $\alpha = 6.2_{-0.9}^{+1.7}$, 90% confidence; all uncertainties and upper-limits are 90% confidence unless otherwise stated) and considerably higher absorption than observed previously from this source or implied by optical observations ($N_{\text{H},22} = 0.50_{-0.10}^{+0.22}$). We reject the model on this basis.

A Raymond-Smith plasma model (Raymond & Smith 1977) with an underlying power law is also statistically acceptable, however, with an abundance limited to $Z < 1.4 \times 10^{-3} Z_{\text{sol}}$.⁹ In addition, it has been shown previously that the X-ray-to-optical flux ratio is substantially greater than is typical for stellar coronal sources (Bildsten & Rutledge 2000). We therefore reject a model which ascribes this emission to the corona of the stellar companion. Though not physically motivated, a thermal bremsstrahlung spectrum acceptably fits the data, with a volume emission measure of $\int n_e n_I dV = 2.3 \times 10^{56} (d/1.2 \text{ kpc}) \text{ cm}^{-3}$ and a temperature of 0.34 keV.

To enable comparison with previous work, we also fit the data with an absorbed blackbody and powerlaw. The best fit with a fixed $N_{\text{H},22} = 0.26$ (Campana et al. 2000) is

⁹While the metallicity of the companion has not been observationally constrained, Martin et al. (1994), while investigating Li abundance, found that the Ca I $\lambda 6717$ line is consistent with solar metallicity, and that an assumed solar Fe abundance in their spectral fits to the Li I doublet is consistent with the data. In optical spectral studies of the companion (Cowley et al. 1988; Chevalier et al. 1989; McClintock & Remillard 1990; McClintock & Remillard 2000), while metal absorption features are observed, the metallicity of the companion is not estimated; however, it does not appear to be so substantially sub-solar.

rejected ($\chi^2_{\nu}=3.1/10$ dof; prob= 5×10^{-4}). With all parameters free, we find $N_{\text{H},22}<0.071$ (90%); $kT_{\text{eff}}=0.175^{+0.012}_{-0.017}$; $r=1.1^{+0.4}_{-0.2}$ ($d/1.2$ kpc) km; $\alpha = 1.2^{+0.4}_{-0.5}$ ($\chi^2_{\nu}=0.75/9$ dof; prob= 0.67).

2.2. Solar Metallicity Atmosphere

We fit the *Chandra* data with a solar metallicity atmospheric model for a 10 km, $1.4M_{\odot}$ NS, with relative abundances given by Grevesse & Noels (1993). A galactic absorption and solar metallicity atmosphere model failed to fit the spectrum ($\chi^2_{\nu}=18/11$ dof), due to the high energy (>2 keV) excess attributed above to the power-law component, and to spectral curvature below 1 keV. With an additional power-law component, the best-fit spectrum is still unacceptable (prob = 3×10^{-8}), largely due to the Fe L edge near 0.534 keV (for a $1.4M_{\odot}$, 10 km NS). While the model atmospheres assume no rotation and are static, the major discrepancy between the model and data is this absorption edge, which will not be significantly altered by these effects.

A solar metallicity NS atmosphere spectrum is therefore strongly rejected. More detailed investigation regarding sub-solar metallicity spectra is in progress, and will be presented in forthcoming work. It would be highly useful to have response matrices refined down to 0.3 keV for this work. These will be valuable limits, as accretion at a rate high enough to explain the quiescent thermal emission would enrich the atmospheric metal content to a detectable level (BBR98).

2.3. Comparison between the *Chandra*, *BeppoSAX* and *ASCA* X-ray spectra

Cen X–4 has been detected on 6 occasions in quiescence, with *Einstein* and *EXOSAT* (Van Paradijs et al. 1987), twice with *ASCA* (Asai et al. 1996b; Asai et al. 1998), once with *ROSAT*/HRI (Campana et al. 1997) and once with *BeppoSAX* (Campana et al. 2000). The measured luminosities and blackbody spectral parameters from the published observations are listed in Table 2.

In this section, we compare the *Chandra* X-ray spectrum with that previously obtained with *BeppoSAX* (Campana et al. 2000) and with the *ASCA*/SIS+GIS spectrum (Asai et al. 1996a; Asai et al. 1998; Rutledge et al. 1999). We do not compare with one other existing *ASCA*/GIS observation as it was performed largely with the GIS, with lower S/N than the first *ASCA* observation, and is comparable to the first *ASCA* observation (Asai et al. 1998). We have previously re-analyzed the *ASCA* observation (Rutledge et al. 1999) and use the same resulting spectrum here.

2.3.1. Re-Analysis of BeppoSAX observation

Campana et al.(2000; C00 hereafter) interpreted the quiescent X-ray spectrum (measured with *ASCA* and *BeppoSAX*) of Cen X–4 as a black-body, and found a mean blackbody radius $3.1_{-3.1}^{+3.7}$ km for the thermal component (the best-fit blackbody radius with *BeppoSAX* data alone was $r=10_{-1.8}^{+10.8}$ km). However, N_{H} was held fixed at the best-fit value of $N_{\text{H},22}=0.26$, which is higher than the optically implied value. We undertook a reanalysis of the *BeppoSAX* observation of Cen X–4, previously analyzed by C00. There are two major differences between our spectral analysis of the LECS data (0.3-2 keV) and theirs:

1. For the LECS background data, C00 used the standard “blank fields” background which are taken from several “blank” areas of the sky (Parmar et al. 1999). However, Cen X–4 is located in a region of the sky with higher than average low-energy background ($l = 332.24$ deg, $b = +23.88$ deg), according to the ROSAT/All-Sky-Survey Soft X-ray Background maps (≈ 0.75 keV; Snowden et al. 1997, Fig 6b). Thus, the “blank fields” background underestimates soft X-ray background in the Cen X–4 observation. We used an alternative method of background estimation described by Parmar et al. (the “annulus” method; 1999), in which the background intensity is assumed to be proportional to the countrate in an annulus in the LECS detector, with a spectrum identical to that found with the “blank fields” method. By this method, the 0.3-1.0 keV background counts account for 60% of the total counts in the Cen X–4 source region, whereas they only account for 34% in the “blank fields” method; the counting uncertainty in the source region is 10%, and therefore this difference in background countrate is significant. As the “annulus” method scales with the local background countrate, it is a more realistic estimation of the local low-energy (<2 keV) background, and so we adopt it.
2. For the LECS data, we used a larger extraction radius than C00 (8' vs. 4'); the LECS point-spread-function becomes broad toward the lower energies (80% encircled energy at 1.5 keV is 3'.0, and at 0.28 keV is 6'.1; the 95% radius is 5'.5 and 8'.5 at 1.5 and 0.28 keV, respectively). The smaller extraction radius used by C00 may have biased the resulting N_{H} upwards. This collected 647 counts from the LECS in 21524 sec (much greater than the 233 counts found by C00). In the 0.3-1.0 keV, there are 84 counts in the source region. We estimate that using an 8' radius instead of a 4' radius increases the observed source countrate by 30%, which is larger than the Poisson uncertainty of 10%.

For the MECS data, we used a 4' extraction radius, which extracted 651 counts (comparable to the 632 found by C00). We used the standard MECS background file

(MECS23_bkg.evt) extracting background counts using the same region as for the source fields. The source background subtracted countrates are $(5.3 \pm 1.6) \times 10^{-3}$ c/s (0.1-3.1 keV) and $(3.3 \pm 0.4) \times 10^{-3}$ c/s (1.7-9.0 keV) in the LECS and MECS instruments, respectively. The LECS data has lower S/N than reported by C00 due to the higher background; we find a slightly higher MECS countrate than found previously.

For comparison with previous work, we fit the *BeppoSAX* LECS+MECS data with an absorbed black-body plus power-law spectrum. We obtained an acceptable fit ($\chi^2_\nu = 0.65/1$ dof; prob=0.42), with the following best-fit parameters: $N_{\text{H},22} < 0.95$, $\alpha = 1.6^{+0.6}_{-0.8}$, $kT_{\text{eff}} = 0.10^{+0.15}_{-0.04}$ keV. We were unable to put any reasonable limits on the BB radius (> 0.4 km, unbounded from above), as the best-fit spectrum merely would increase the column density to compensate for larger and larger areas. When we hold the column density fixed at the best-fit value, we find $r_{\text{BB}} = 7^{+26.3}_{-6.5}$ km; when we hold the column density fixed at the optically implied value ($N_{\text{H},22} = 0.055$), we find $r_{\text{BB}} = 2^{+5}_{-1.6}$ km. These values are comparable to those found with *ASCA* (Asai et al. 1996b; Rutledge et al. 1999), and below those found by C00. We attribute this difference to our more accurate background subtraction and larger extraction radius for the LECS data. The unabsorbed total flux is 2.7×10^{-12} erg cm $^{-2}$ s $^{-1}$ (4.7×10^{32} erg s $^{-1}$, 0.5-10.0 keV); the unabsorbed flux of the BB component is 2.2×10^{-12} erg cm $^{-2}$ s $^{-1}$ (0.5-10.0 keV), and of the power-law component it is 0.44×10^{-12} erg cm $^{-2}$ s $^{-1}$ (0.5-10.0 keV). As we find in the next section, the *BeppoSAX* and *Chandra* spectra (and their corresponding fluxes) are, within statistics, the same.

2.3.2. Joint Spectral Fitting of *Chandra*, *BeppoSAX* and *ASCA* X-ray Spectra

We performed a joint spectral fit of the *Chandra*, *ASCA*, and *BeppoSAX* data. We assumed a 4% systematic uncertainty in the detector responses for all instruments, and held N_{H} fixed at its optically implied value. We used an absorbed H atmosphere+powerlaw spectrum. The best spectral fit rejects a single model to account for all three observed spectra ($\chi^2_\nu = 3.3/53$ dof; prob= 5×10^{-15}). A joint *Chandra/BeppoSAX* fit provided a statistically acceptable fit, indicating that the *Chandra* and *BeppoSAX* spectra are statistically identical. A joint *Chandra/ASCA* fit was not acceptable. The *ASCA* data are, by themselves, acceptably fit by this same assumed spectrum (Rutledge et al. 1999).

We jointly fit the *Chandra* and *ASCA* spectra, permitting one of the five parameters (kT , r , α , and power-law normalization N_α) to be different between the two spectra, each in turn. None of these fits are formally statistically acceptable. However, while a change in α is soundly rejected (prob $\leq 4 \times 10^{-10}$), and a change in r is of low probability (prob = 0.001), changes in the N_α or kT are found to be marginal (both prob = 0.01). This is in

the range where systematic uncertainty in the detector responses (in particular, the area as a function of energy) become important. For example, if we increase the systematic uncertainty from 4% to 8% (which, for example, could be due to a systematic offset in the absolute flux calibrations between the two detectors), the best fits for a changing N_α or kT become statistically acceptable.

Thus, while the *Chandra* and *ASCA* spectra are significantly different, we cannot unequivocally state whether this difference is due to a change in the N_α or the kT , a combination of these with other parameters, or a systematic difference between the absolute calibrations of the two instruments. However, we provide the best-fit spectral parameters in Table 3, for a changing power-law normalization and thermal temperature. These then serve as an upper-limit for variability in these parameters between the two observations. Between the *Chandra* and *ASCA* epochs, then, we find that the thermal temperature decreased (at most) from $kT = 0.085$ to 0.077 keV; or the power-law normalization decreased from 15.2×10^{-5} to 5.9×10^{-5} phot cm $^{-2}$ s $^{-1}$ at 1 keV. Moreover, the interpretation of these spectra impacts the best-fit power-law slope, which is $\alpha = 1.0$ if it is the temperature which changes, or $\alpha = 1.7$ if it is the normalization which changes.

Finally, we fit a spectral model to the *Chandra*, *BeppoSAX*, and *ASCA* data assuming that the power-law slope and flux changes, but that the thermal component does not. The resulting best-fit parameters and uncertainties are shown in Table 4. The best-fit is statistically acceptable. The power-law component (taken to be the same for the *Chandra* and *BeppoSAX* observations) is flatter in the *Chandra+BeppoSAX* observations than during the *ASCA* observation (1.0 ± 0.4 vs. 1.9 ± 0.3), and has a lower flux, by about a factor of two.

We also fit these spectra assuming that the thermal r and kT vary while the power-law component does not (although this is not theoretically motivated). An acceptable fit is found ($\chi^2_\nu = 1.33/52$ dof; prob=0.06), with *Chandra+BeppoSAX* values of ($r = 13.4^{+4.2}_{-2.4}$ km, $kT = 0.074^{+0.006}_{-0.008}$ keV) and *ASCA* values of ($r = 7.1^{+2.5}_{-3.0}$ km, $kT = 0.10^{+0.026}_{-0.009}$ keV).

2.4. Intensity Variability

Variability in the luminosity of Cen X–4 has been observed over timescales from days to years. Van Paradijs et al. (1987, JVP87 hereafter) detected Cen X–4 using *EXOSAT*/LE1 with the CMA instrument and LEXAN 3000 Å filter (Taylor et al. 1981), with a countrate of $(5.4 \pm 1.2) \times 10^{-3}$ c/s. JVP87 assumed a thermal bremsstrahlung spectrum with temperature between 1 and 5 keV and a column density $N_{\text{H},22} = 0.066$, which,

for this countrate, corresponded to a flux at earth of $(2.2-5.6) \times 10^{-12}$ erg s⁻¹ cm⁻². Using the same assumptions with an earlier *Einstein*/IPC observation, they found a flux at earth between $(1.1-1.5) \times 10^{-12}$ erg s⁻¹ cm⁻², concluding that the X-ray luminosity must have increased between the Einstein and *EXOSAT* observations by 50-500%. Campana et al. (1997) measured a flux variation of a factor of 3 in <4 days using *ROSAT*/HRI.

We started by looking for variability during our observation. We first separated the data into two energy bins: pulse-invariant (PI) bins 2-136 (0.2-2 keV) and PI bins >136 (>2 keV). We included PI bins in which the area and energy calibration is presently not reliable; while these are not useful (presently) for flux and spectral calculations, they can be used for investigations in variability.

There were a total of $N_{\text{phot}} = 2553$ counts in PI bins 2-136 ($\approx 0.2-2$ keV). We used 23903 time bins which were 0.44104 sec in length which each had exposure of only 0.40 sec, for a total observation time of $T_{\text{obs}} = 10542$ sec. We performed a Fourier transform, producing a power density spectrum (PDS) of 11951 frequency bins across the 0.0001-1.13 Hz frequency range, normalized according to Leahy et al. (1983). We logarithmically rebinned this data, and fit the PDS with functions $P(\nu)$, to extract the integrated r.m.s power. The PDS is acceptably described as counting noise (constant power of 2.0; $\chi^2_{\nu} = 1.41/16$ dof; prob=0.13); we therefore observe no variability in this data. Using a power-law distribution with the slope of $\alpha = 1$ held fixed, with an underlying Poisson level ($P = 2$) also held fixed, we find a 3σ upper limit on the root-mean-square variability of <18% (0.0001-1 Hz). For a flat power-law ($\alpha = 0$), the 3σ upper limit is <10%.

There are a total of 151 counts in PI bins >136 ($\gtrsim 2.0$ keV) in this observation. We performed an identical PDS analysis as for the low energy counts, although in the fit to the PDS we held the exponent fixed at $\alpha = 1.0$ (producing an acceptable fit; $\chi^2_{\nu} = 1.46/15$ dof). The 3σ upper-limit to the RMS variability >2.0 keV is <50% (0.0001-1 Hz).

We also looked for longer term variability by investigating the hypothesis that the *Chandra* and *ASCA* spectra were identical in all parameters, but different in absolute normalization. We found that the spectra were describable in this way ($\chi^2_{\nu} = 1.05/47$ dof; prob=0.37), with the *ASCA* spectrum a factor 1.65 ± 0.12 (90% uncertainty) more luminous than the *Chandra* spectrum. We interpret this as fitting a well-constrained spectrum from *Chandra* (signal-to-noise ratio S/N ≈ 100) to the low S/N data of *ASCA* (S/N ≈ 4). This provides a rough measure of the luminosity difference between the *ASCA* and *Chandra* observations – a decrease of $40 \pm 8\%$ over 4.9 yr.

3. Summary, Conclusions and Implications

We have analyzed the X-ray spectrum and intensity variability of Cen X–4 observed with *Chandra*, and compared it with earlier observations by *ASCA* and *BeppoSAX*. The *Chandra* X-ray spectrum is inconsistent with all single component models we applied, requiring at least a two component model, with a power-law component that dominates the spectrum above 2 keV and a softer (most likely thermal) component which dominates the spectrum below this energy. The intensity variability during the *Chandra* observation is $<18\%$ (3σ) on timescales between 1-10,000 sec in the 0.2-2.0 keV energy band dominated by the thermal component. The limit on variability is weaker above 2 keV ($<50\%$ r.m.s., 3σ).

Cen X-4’s luminosity decreased between the *ASCA* and *Chandra* observations (4.9 yrs) by $40\pm 8\%$ (0.5-10.0 keV). We attribute this variation to changes in the power-law component. This is comparable to the factor of ~ 3 decrease found over a few days by Campana et al. (1997). We cannot statistically exclude that the power-law component remains constant, and the thermal component varies. Thus, Cen X–4 is variable in quiescence on timescales longer than hours.

3.1. The Thermal Component

Rutledge et al. (1999; 2000) have shown that the soft emission seen in all NS transients in quiescence is best explained as thermal emission from a pure hydrogen NS atmosphere. We have found the same in this *Chandra* observation. Indeed, comparing X-ray spectra taken with *Chandra*, *ASCA* and *BeppoSAX* at different times over 4.9 years, we find that this thermal component is consistent with being constant, with a best-fit radius of $r=12.9\pm 2.6$ ($d/1.2\text{kpc}$) km, and a temperature $kT=0.076\pm 0.007$ keV. These results improve the precision of the quiescent spectrum by a factor of ~ 3 over previous work (Rutledge et al. 1999). We place an upper-limit on the amount of temperature variability across 4.9 years of $\lesssim 10\%$ (Table 3). The agreement between this radius and that measured during Type I X-ray bursts from other systems is strong confirmation that the emitting area is the NS surface.

Two energy sources for the thermal emission have been discussed: accretion in quiescence at a low-rate (Van Paradijs et al. 1987; Menou et al. 1999) and re-emission of heat deposited into the crust during the large accretion events (BBR98). The required accretion rate for the bolometric luminosity of 7×10^{32} erg s $^{-1}$ is $\dot{M}_q \approx 6 \times 10^{-14} M_\odot \text{ yr}^{-1}$, adequate to keep the metal content in the atmosphere comparable or larger than that in

the accreting material (Bildsten et al. 1992). If the metal content in the accreting material is very sub-solar (that is, effectively pure hydrogen), accretion at these rates would give thermal emission much like we observe (Zampieri et al. 1995). However, solar metallicity accretion is likely ruled out, largely due to the lack of absorption from the Fe L edge near 0.5 keV. Tighter constraints on the photospheric metallicity will be the subject of future work with these data and will allow us to more thoroughly constrain the active accretion hypothesis, which does not have a specific way of predicting \dot{M}_q .

The other possible mechanism is re-emission of heat deposited in the inner crust due to pycnonuclear reactions, electron captures and neutron emissions (Haensel & Zdunik 1990) during accretion events (BBR98). The layers where this heat is deposited are in close thermal contact with the NS core. The reactions then heat the core to a temperature of $\sim 10^8$ K over $\sim 10^4$ yr (BBR98; Colpi et al. 2001). The NS reaches an equilibrium where the time averaged nuclear heating equals the quiescent thermal emission, $L_q \approx (1 \text{ MeV/nucleon})\langle\dot{M}\rangle$, implying a time averaged accretion rate for this NS of $\langle\dot{M}\rangle \approx 10^{-11} M_\odot \text{ yr}^{-1}$.

We can compare this $\langle\dot{M}\rangle$ to that implied by the outbursts. The outburst in 1969 had a total fluence of $\approx 3 \text{ ergs cm}^{-2}$ (Chen et al. 1997). There has not been another large outburst of this magnitude recorded since; the small outburst in 1979 had a fluence two orders of magnitude smaller. It is uncertain to measure the time-averaged accretion rate on the basis of a single outburst. If a large outburst like that in 1969 occurs every 100 years, the time-averaged accretion flux would be $\approx 10^{-9} \text{ ergs cm}^{-2} \text{ s}^{-1}$, which at the 1.2 kpc distance gives $\langle\dot{M}\rangle \approx 10^{-11} M_\odot \text{ yr}^{-1}$, comparable to that implied by the level of the quiescent thermal emission. However, this is a low accretion rate for a binary at this long orbital period, where the likely driver of mass transfer is nuclear evolution of the binary (see Webbink et al. 1983). So, this is an outstanding puzzle for this source. If outbursts like that seen in 1969 occur more frequently than 100 years, the time averaged accretion rate would be higher and in conflict with that implied by the quiescent thermal emission through the mechanism of BBR98, unless the fraction of deposited energy re-emitted as photons is much less than unity. Possible solutions to this, involving enhanced neutrino emission from the core, have been proposed by Colpi et al. (2001) and Ushomirsky & Rutledge (2001).

If the thermal emission is due to a hot neutron star core, then the measured effective temperature of $0.076 \pm 0.007 \text{ keV}$ tells us the internal NS temperature. For example, if the outer layer consists of light elements to a density $6 \times 10^5 \text{ g cm}^{-3}$, then using the fit of Potekhin et al. (1997), we find $T_{\text{core}} = (5.1_{-1.1}^{+1.2}) \times 10^7 \text{ K}$. For these core temperatures, the modified URCA neutrino luminosity is orders of magnitude less than the photon luminosity. The NS core would not be in a thermal steady-state if pion condensation occurs, as the resultant neutrino luminosity (Umeda et al. 1994) would be much larger than

the heating supplied by reactions in the deep crust. As a result, if some enhanced cooling mechanism were operating in the core, then we would expect $T_{\text{core}} \lesssim 10^7$ K and the crust and surface temperature should be decreasing on a timescale of ~ 1 yr (BBR98; Ushomirsky & Rutledge 2001).

The lack of luminosity variability in general, and the stability of the thermal component over a ~ 5 year timescale supports the model proposed by BBR98 for the thermal component. It remains to be unequivocally demonstrated, however, that the variability observed is restricted to the power-law component, and that the variability of the temperature of the thermal component is limited to $\lesssim 1\%$, as expected from variations in the T_{core} from outburst to outburst (Colpi et al. 2001).

3.2. The Power-Law Spectral Component

The origin of the hard power-law component remains unclear. Many ideas have been put forward, ranging from emission due to an active pulsar wind colliding with the accretion disk, x-ray emission from a turned-on radio pulsar (Stella et al. 1994) and accretion onto the magnetosphere (for a review, see Campana et al. 1998a).

There is no direct knowledge of either the NS spin or magnetic field in Cen X-4, though the presence of Type I bursts points to $B < 10^{10}G$. None of the above models make specific predictions about either the level of emission or its spectral shape which explain the present observations.

Moreover, the limitation to $< 1\%$ rms of coherent intensity pulsations in the transiently accreting NS Aql X-1 (another transient, type-I X-ray bursting source) following a rapid decrease in flux (Chandler & Rutledge 2000) which was interpreted as due to magnetic inhibition of the accretion flow (Campana et al. 1998b; Zhang et al. 1998) does not support the idea that accretion onto the compact object is ultimately restricted by a “propeller effect”, favoring instead an interpretation of the end of transient outbursts as due to an end of the disk instability, such as occurs in dwarf novae (King & Ritter 1998). In fact, abrupt declines in dwarf novae outburst fluxes are observed, and are explained within the disk instability model (Cannizzo 1994), without invoking magnetic inhibition. The absence, then, of a magnetosphere in transiently accreting NSs would preclude attributing the power-law to magnetospheric accretion, and energy production would have to be attributed to another site within the NS binary system.

Spectral comparison between the *ASCA* and *Chandra* observation indicate that a change in (only) the power-law normalization is marginally acceptable, and therefore that a

change in the spectral slope (from $\alpha = 1.9 \pm 0.3$ to $\alpha = 1.0 \pm 0.4$) is also required. It is unclear how a change in the spectral slope could be produced while limiting the luminosity decrease to less than a factor of three in any of the proposed emission mechanisms (Campana et al. 1998a).

There might be some help in understanding the power-law component from other wavelength bands, where it was found recently that, in quiescence, the energy density (νF_ν) is nearly flat from UV through the X-ray energy range, in marked contrast to A0620-00, in which the energy density falls in the UV band (McClintock & Remillard 2000). This flat-spectrum has been interpreted as due to a shock at the splash-point of accretion from the companion (Menou & McClintock 2001). However, while we also find a flat spectrum for the *ASCA* observation (photon power-law slope of $\alpha = 1.9 \pm 0.4$) we find an *increasing* energy density during the *Chandra* observation ($\alpha = 1.0 \pm 0.4$). Clearly, further observational study of the power-law component is required to understand even its most basic aspects.

3.3. Future Work on Neutron Star Radii from Thermal Emission

The dominant systematic uncertainty in the measurement of the radius of the neutron star in Cen X-4 is the distance to the object. This will be dramatically improved by the Space Interferometric Mission, which can measure the parallax of the 18.^m5 counterpart to $\sim 10 \mu\text{asec}$, or $<1\%$ distance uncertainty at 1.2 kpc. This would make N_{H} the dominant uncertainty in the measured thermal emission radius, followed by any systematic uncertainty in the modelled spectrum. For example, a planned 50 ksec XMM observation will permit constraint of r/D to $\sim 2\%$ while simultaneously measuring N_{H} .

It has been suggested that some fraction of the low-luminosity X-ray sources in globular clusters are transiently accreting NSs in quiescence (Verbunt et al. 1984; Rutledge et al. 2000). These make excellent targets for NS radius measurements, as there are multiple objects per observing field, all at the same distance and interstellar column density (BBR98). *Chandra* imaging observations of globular clusters (Grindlay et al. 2000; Pooley et al. 2000) indicate source densities in excess of several per square arcmin (down to luminosities of $L_X \sim 10^{30} \text{ erg s}^{-1}$) with over 100 X-ray sources in the core of 47 Tuc alone. It is still unanswered as to what fraction of these are quiescent NS's. The high source density will complicate X-ray spectroscopy with XMM or *Con-X* (with angular resolution $\sim 15''$), making *Chandra* imaging spectroscopy the best way to pursue this science.

The authors are grateful to the *Chandra* Observatory team for producing this exquisite

observatory. R.R. thanks Andy Fabian for a useful conversation regarding historical measurements of photospheric absorption lines. The authors thank Dany Page and Andrew Cumming for comments on the text prior to submission. This research was partially supported by the National Science Foundation under Grant No. PHY99-07949 and by NASA through grant NAG 5-8658, NAG 5-7017 and the *Chandra* Guest Observer program through grant NAS 8-39073. L. B. is a Cottrell Scholar of the Research Corporation. E. F. B. acknowledges support from an Enrico Fermi Fellowship.

REFERENCES

- Arnaud, K. A., 1996, in G. Jacoby & J. Barnes (eds.), *Astronomical Data Analysis Software and Systems V.*, Vol. 101, p. 17, ASP Conf. Series
- Asai, K., Dotani, T., Hoshi, R., Tanaka, Y., Robinson, C. R., & Terada, K., 1998, PASJ 50, 611
- Asai, K., Dotani, T., Kunieda, H., & Kawai, N., 1996a, PASJ 48, L27
- Asai, K., Dotani, T., Mitsuda, K., Hoshi, R., Vaughan, B., Tanaka, Y., & Inoue, H., 1996b, PASJ 48, 257
- Bildsten, L. & Rutledge, R. E., 2000, ApJ 541, 908
- Bildsten, L., Salpeter, E. E., & Wasserman, I., 1992, ApJ 384, 143
- Bildsten, L., Salpeter, E. E., & Wasserman, I., 1993, ApJ 408, 615
- Blair, W. P., Raymond, J. C., Dupree, A. K., Wu, C. C., Holm, A. V., & Swank, J. H., 1984, ApJ 278, 270
- Brown, E. F., Bildsten, L., & Rutledge, R. E., 1998, ApJ 504, L95, [BBR98]
- Campana, S., Colpi, M., Mereghetti, S., Stella, L., & Tavani, M., 1998a, A&A Rev. 8, 279
- Campana, S., Mereghetti, S., Stella, L., & Colpi, M., 1997, A&A 324, 941
- Campana, S., Stella, L., Mereghetti, S., Colpi, M., Tavani, M., Ricci, D., Fiume, D. D., & Belloni, T., 1998b, ApJ 499, L65
- Campana, S., Stella, L., Mereghetti, S., & Cremonesi, D., 2000, A&A 358, 583
- Canizares, C. R., McClintock, J. E., & Grindlay, J. E., 1980, ApJ 236, L55
- Cannizzo, J. K., 1994, ApJ 435, 389
- Chandler, A. & Rutledge, R. E., 2000, ApJ, in press
- Chen, W., Shrader, C. R., & Livio, M., 1997, ApJ 491, 312
- Chevalier, C., Ilovaisky, S. A., Van Paradijs, J., Pedersen, H., & Van der Klis, M., 1989, A&A 210, 114
- Colpi, M., Geppert, U., Page, D., & Possenti, A., 2001, ApJ, submitted, astro-ph/001572

- Cowley, A. P., Hutchings, J. B., Schmidtke, P. C., Hartwick, F. D. A., Crampton, D., & Thompson, I. B., 1988, *AJ* 95, 1231
- Damen, E., Jansen, F., Penninx, W., Oosterbroek, T., van Paradijs, J., & Lewin, H. G., 1989, *MNRAS* 237, 523
- Damen, E., Magnier, E., Lewin, W. H. G., Tan, J., Penninx, W., & van Paradijs, J., 1990, *A&A* 237, 103
- Day, C. S. R., Fabian, A. C., & Ross, R. R., 1992, *MNRAS* 257, 471
- Foster, A. J., Fabian, A. C., & Ross, R. R., 1987, *MNRAS* 228, 259
- Garcia, M. R., 1994, *ApJ* 435, 407
- Garcia, M. R. & Callanan, P. J., 1999, *AJ* 118, 1390
- Gorenstein, P., 1975, *ApJ* 198, 95
- Grevesse, N. & Noels, A., 1993, in E. Prantzos, M. Vaugioni-Flam, & M. Gasse (eds.), *Origin and Evolution of the Elements*, p. 14, Cambridge University Press
- Grindlay, J., Edmonds, P., Heinke, C., & Murray, S., 2000, *AAS/High Energy Astrophysics Division* 32, 4505
- Haensel, P. & Zdunik, J. L., 1990, *A&A* 227, 431
- Hertz, P. & Grindlay, J. E., 1983, *ApJ* 267, L83
- Kaaret, P., Ford, E. C., & Chen, K., 1997, *ApJ* 480, L27
- King, A. R. & Ritter, H., 1998, *MNRAS* 293, L42
- Kluźniak, W., 1998, *ApJ* 509, L37
- Kluźniak, W., Michelson, P., & Wagoner, R. V., 1990, *ApJ* 358, 538
- Leahy, D. A., Darbro, W., Elsner, R. F., Weisskopf, M. C., Kahn, S., Sutherland, P. G., & Grindlay, J. E., 1983, *ApJ* 266, 160
- Lewin, W., Van Paradijs, J., & Taam, R., 1993, *Space Sci. Rev.* 62, 223
- London, R. A., Howard, W. M., & Taam, R. E., 1986, *ApJ* 306, 170
- Madej, J., 1990, *Acta Astronomica* 40, 223

- Madej, J., 1991, *ApJ* 376, 161
- Magnier, E., Lewin, W. H. G., van Paradijs, J., Tan, J., Penninx, W., & Damen, E., 1989, *MNRAS* 237, 729
- Martin, E. L., Rebolo, R., Casares, J., & Charles, P. A., 1994, *ApJ* 435, 791
- McClintock, J. E. & Remillard, R. A., 1990, *ApJ* 350, 386
- McClintock, J. E. & Remillard, R. A., 2000, *ApJ* 531, 956
- Menou, K., Esin, A. A., Narayan, R., Garcia, M. R., Lasota, J. P., & McClintock, J. E., 1999, *ApJ* 520, 276
- Menou, K. & McClintock, J. E., 2001, *ApJ*, submitted, astro-ph/0010430
- Nakamura, N., Inoue, H., & Tanaka, Y., 1988, *PASJ* 40, 209
- Paerels, F., 1997, *ApJ* 476, L47
- Parmar, A. N., Oosterbroek, T., Orr, A., Guainazzi, M., Shane, N., Freyberg, M. J., Ricci, D., & Malizia, A., 1999, *A&AS* 136, 407
- Pavlov, G. G. & Shibanov, I. A., 1978, *Soviet Astronomy* 22, 214
- Pavlov, G. G., Shibanov, I. A., & Zavlin, V. E., 1991, *MNRAS* 253, 193
- Pooley, D., Lewin, W. H. G., Verbunt, F., Fox, D. W., Margon, B., Kaspi, V. M., van der Klis, M., & Miller, J., 2000, *AAS/High Energy Astrophysics Division* 32, 2901
- Potekhin, A. Y., Chabrier, G., & Yakovlev, D. G., 1997, *A&A* 323, 415
- Predehl, P. & Schmitt, J. H. M. M., 1995, *A&A* 293, 889
- Rajagopal, M. & Romani, R. W., 1996, *ApJ* 461, 327
- Raymond, J. C. & Smith, B. W., 1977, *ApJS* 35, 419
- Rutledge, R. E., Bildsten, L., Brown, E. F., Pavlov, G. G., & Zavlin, V. E., 1999, *ApJ* 514, 945
- Rutledge, R. E., Bildsten, L., Brown, E. F., Pavlov, G. G., & Zavlin, V. E., 2000, *ApJ* 529, 985
- Snowden, S. L., Egger, R., Freyberg, M. J., McCammon, D., Plucinsky, P. P., Sanders, W. T., Schmitt, J. H. M. M., Truemper, J., & Voges, W., 1997, *ApJ* 485, 125

- Stella, L., Campana, S., Colpi, M., & Mereghetti, S. andx Tavani, M., 1994, *ApJ* 423, L47
- Tanaka, Y. & Lewin, W., 1995, in W. Lewin, J. Van Paradijs, & E. Van Den Heuvel (eds.), *X-Ray Binaries*, Vol. 1, p. 126, Cambridge University Press
- Tanaka, Y. & Shibazaki, N., 1996, *ARA&A* 34, 607
- Taylor, B. G., Andresen, R. D., Peacock, A., & Zobl, R., 1981, *Space Science Reviews* 30, 479
- Thorsett, S. E. & Chakrabarty, D., 1999, *ApJ* 512, 288
- Titarchuk, L., 1994, *ApJ* 429, 340
- Umeda, H., Nomoto, K., Tsuruta, S., Muto, T., & Tatsumi, T., 1994, *ApJ* 431, 309
- Ushomirsky, G. & Rutledge, R. E., 2001, in preparation
- Van Paradijs, J., 1982, *A&A* 107, 51
- Van Paradijs, J. & Lewin, W. H. G., 1987, *A&A* 172, L20
- Van Paradijs, J., Verbunt, F., Shafer, R. A., & Arnaud, K. A., 1987, *A&A* 182, 47
- Verbunt, F., Bunk, W., Hasinger, G., & Johnston, H. M., 1995, *A&A* 300, 732
- Verbunt, F., Elson, R., & Van Paradijs, J., 1984, *MNRAS* 210, 899
- Waki, I., Inoue, H., Koyama, K., Matsuoka, M., Murakami, T., Ogawara, Y., Ohashi, T., Tanaka, Y., Hayakawa, S., Tawara, Y., Miyamoto, S., Tsunemi, H., & Kondo, I., 1984, *PASJ* 36, 819
- Webbink, R. F., Rappaport, S., & Savonije, G. J., 1983, *ApJ* 270, 678
- Zampieri, L., Turolla, R., Zane, S., & Treves, A., 1995, *ApJ* 439, 849
- Zavlin, V. E., Pavlov, G. G., & Shibanov, Y. A., 1996, *A&A* 315, 141
- Zhang, S. N., Yu, W., & Zhang, W., 1998, *ApJ* 494, L71
- Zhang, W., Strohmayer, T. E., & Swank, J. H., 1997, *ApJ* 482, L167

Fig. 1.— The νF_ν model spectrum of Cen X-4, and the observed *Chandra*/ACIS-S BI data above 0.5 keV. The solid line is the best-fit *unabsorbed* H-atmosphere plus power-law model spectrum with $N_{\text{H},22}=0.055$ held fixed (that is, the intrinsic X-ray spectrum of Cen X-4, prior to absorption by the inter-stellar medium; see Table 1). The dashed line is the model power-law component, and the dashed-dotted line is the H-atmosphere component. The two spectral components are equal near ≈ 2 keV, above which the power-law component dominates, and below which the H atmosphere component dominates. The H atmosphere spectral parameters are $r = 13.3^{+2.4}_{-3.9}$ km, and $kT = 0.074^{+0.012}_{-0.005}$ keV. The power-law component is rising in νF_ν . The crosses are the observed *Chandra* data, with error-bars in countrate.

Cen X-4: Chandra ACIS-S/BI, June 23 2000

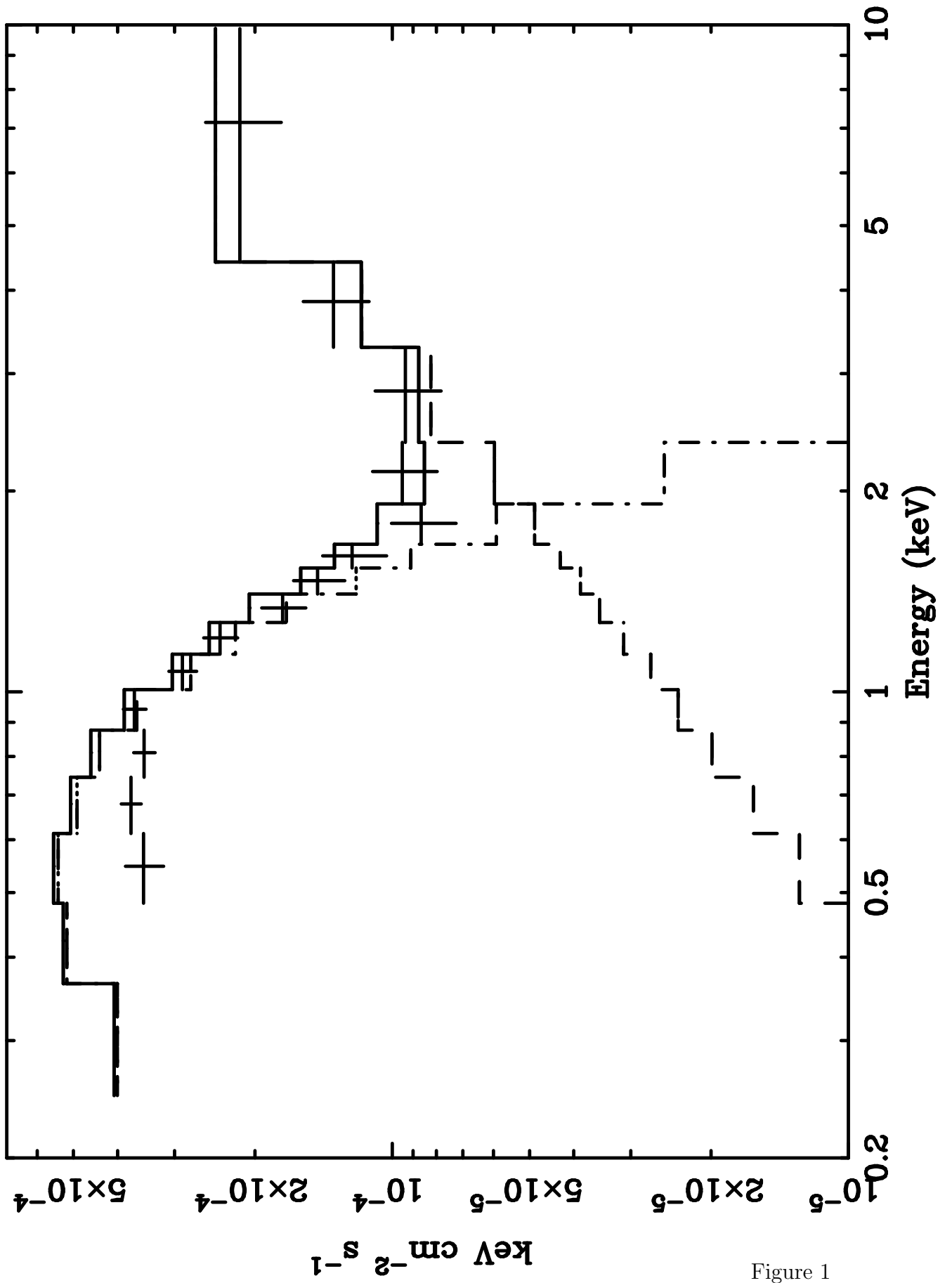


Figure 1

Table 1. *Chandra* Observation
Spectral Parameters (0.5-10 keV)

H Atmosphere + Power-Law	
$N_{\text{H},22}$	$0.10^{+0.10}_{-0.07}$
α	1.0 ± 0.4
$F_{\text{X,PL}}$	5
kT (keV)	0.067 ± 0.019
r	19^{+45}_{-10}
Total Model Flux	13
χ^2_{ν}/dof (prob)	0.94/9 (0.49)
H Atmosphere + Power-Law (N_{H} fixed)	
$N_{\text{H},22}$	(0.055)
α	$1.0^{+0.6}_{-0.4}$
$F_{\text{X,PL}}$	4.6
kT (keV)	$0.074^{+0.012}_{-0.005}$
r	$13.3^{+2.4}_{-3.9}$ km
Total Model Flux	11.3
χ^2_{ν}/dof (prob)	0.83/10 (0.50)

Note. — X-ray fluxes are un-absorbed, in units of 10^{-13} erg cm $^{-2}$ s $^{-1}$ (0.5-10 keV). Assumed source distance $d=1.2$ kpc.

Table 2. Cen X–4 Quiescent Observations

Ref.	Obs Date Instrument	kT_{BB}	X-ray Luminosity (passband)	α	$N_{H,22}$
1	1980 Jul 28 <i>Einstein</i> /IPC	$0.32^{+0.12}_{-0.08}$	$2\text{-}3 \times 10^{32}$ (0.5-4.5 keV)	...	0.066
1	1986 Feb 21 <i>EXOSAT</i> /CMA	...	$4\text{-}11 \times 10^{32}$ (0.5-4.5 keV)	...	0.066
2	1994 Feb 27-28 <i>ASCA</i> /SIS+GIS	$0.16^{+0.03}_{-0.02}$	$4^{+4}_{-1.7} \times 10^{32}$ (0.5-10 keV)	1.9 ± 0.3	< 0.2
3	1995 Aug 16-26 <i>ROSAT</i> /HRI	...	7×10^{31} (0.1-2.4 keV)
4	1997 Feb 4-5 <i>ASCA</i> /GIS	0.13 ± 0.02	$3^{+3}_{-2} \times 10^{32}$ (0.5-10 keV)	2.5 ± 0.5	0.3 ± 0.1
5	1999 Feb 9 SAX/LECS+MECS		(see discussion of § 2.3.1) (0.5-10 keV)		
6	2000 June 23 <i>Chandra</i> /ACIS-S	$0.176^{+0.012}_{-0.015}$	1.7×10^{32} (0.5-10 keV)	$1.2^{+0.4}_{-0.5}$	< 0.06

Note. — The quoted luminosity is the luminosity at the source (i.e. – unabsorbed, using the column density noted). Assumed source distance $d=1.2$ kpc; luminosities quoted from references which assumed different distances have been changed.

References. — 1, Van Paradijs et al. 1987; 2, Asai et al. 1996b; 3, Campana et al. 1997; 4, Asai et al. 1998; 5, Campana et al. 2000; 6, present work.

Table 3. H Atmosphere+Power Law Spectral Parameters of *Chandra*/ACIS and *ASCA*/SIS+GIS

N_H (10^{22} cm $^{-2}$)	α	$F_{X,PL}^b$	kT (keV)	r (km) ($\frac{d}{1.2\text{kpc}}$)	Variable Parameter	<i>Chandra</i> Value	<i>ASCA</i> Value	χ^2_{ν}/dof	prob.
(0.055)	1.0 ± 0.4	$5.7^{+1.0}_{-2.4}$...	$12^{+3.0}_{-2.4}$	kT	0.077 ± 0.007	$0.085^{+0.008}_{-0.007}$	1.5/47	0.01
(0.055)	$1.7^{+0.4}_{-0.2}$...	$0.076^{+0.005}_{-0.010}$	$12^{+5}_{-1.3}$	$F_{X,PL}$	$3.5^{+1.6}_{-0.9}$	$9.1^{+3.1}_{-2.1}$	1.5/47	0.01

Note. — ^bPower-law fluxes are unabsorbed (0.5-10.0 keV), in units of 10^{-13} erg cm $^{-2}$ s $^{-1}$; Values in parenthesis are held fixed.

Table 4. H Atmosphere+Power Law Spectral Parameters of *Chandra*/ACIS,
BeppoSAX/LECS+MECS and *ASCA*/SIS+GIS

N_{H} (10^{22} cm $^{-2}$)	kT (keV)	r (km) ($\frac{d}{1.2\text{kpc}}$)	<i>Chandra + BeppoSAX</i>		<i>ASCA</i>		χ^2_{ν}/dof	prob.
			α	$F_{\text{X,PL}}^b$	α	$F_{\text{X,PL}}^b$		
(0.055)	0.076 \pm 0.007	12.9 \pm 2.6	1.0 \pm 0.4	4.4 $^{+1.9}_{-2.3}$	1.9 \pm 0.3	8.6 \pm 1.6	1.0/52	0.43

Note. — ^bPower-law fluxes are unabsorbed (0.5-10.0 keV), in units of 10^{-13} erg cm $^{-2}$ s $^{-1}$; Values in parenthesis are held fixed.